Simulation of high Schmidt number fluids with dissipative particle dynamics: Parameter identification and robust viscosity evaluation

Terms of use:

(Article begins on next page)

23 April 2024

Simulation of high Schmidt number fluids with dissipative particle dynamics: Parameter identification and robust viscosity evaluation

N. Lauriello,[1] J. Kondracki,[1] A. Buffo,[1, a)] G. Boccardo,[2] M. Bouaifi,[2] M. Lisal,[3, 4] and D. Marchisio[1]

[1)]*DISAT – Institute of Chemical Engineering, Politecnico di Torino,*
C.so Duca degli Abruzzi 24, Torino 10129, Italy

[2)]*Centre de Recherche et d'Innovation de Lyon, Solvay, 85 Avenue des Frères Perret,*
BP 62, Saint-Fons Cedex, 69192, France

[3)]*Department of Molecular and Mesoscopic Modelling, The Czech Academy of Sciences,*
Institute of Chemical Process Fundamentals, Prague, Czech Republic

[4)]*Department of Physics, Faculty of Science, J. E. Purkinje University, Ústí n. Lab,*
Czech Republic

(Dated: 14 June 2021)

Dissipative particle dynamics (DPD) is a widely used coarse-grained technique for the simulation of complex fluids. Although the method is capable of describing the hydrodynamics of any fluid, the common choice of DPD parameters, such as friction coefficient γ, dissipative cutoff radius r_c^D, coarse-graining factor N_m and weighting function exponent s, unrealistically leads to the simulation of liquid water with a low Schmidt number Sc at standard pressure and temperature. In this work we explored the influence of these parameters, finding the set of parameters needed to properly simulate liquid water. Particular attention was devoted to the numerical techniques to calculate the transport properties from equilibrium simulations, especially in the calculation of the viscosity, comparing the most commonly adopted techniques and formulating a recipe that can be used for further investigations.

[a)]Author to whom correspondence should be addressed: antonio.buffo@polito.it.

I. INTRODUCTION

Multiscale modeling is attracting more and more attention in chemical engineering as it allows to account for phenomena occurring at different length- and time-scales. Because of that, numerous simulation techniques have been developed during the past decades and successfully used in theoretical studies and practical investigations, ranging from the simulation of polyurethane foams[1–3] to the modelling of polymer particle flash nano-precipitation (or solvent displacement)[4]. In these works a continuum modelling technique, such as computational fluid dynamics (CFD) is often coupled with a particle-based molecular/mesoscopic modelling approach. Because of the scale separation the coupling is however performed off-line and only coarse-grain (CG) methods allow, given the average computational resources available nowadays, to perform on-line, on-the-fly, tight coupling. Due to their potential scale-bridging role, CG methods are now more and more popular in many engineering applications, such as for example self-assembly of surfactants[5] and polymers[6,7], modeling of binary mixtures[8], macromolecular dynamics[9,10] or mixing in structured fluids[11].

One of the CG methods, which will be further described and used in this paper, is dissipative particle dynamics (DPD), introduced originally by Hoogerbrugge and Koelman[12] and later on developed by Español and Warren[13]. The main idea behind DPD is to reduce the number of degrees of freedom in the system by grouping several atoms or molecules into single beads, having no hard sphere-like cores anymore. A soft, conservative potential between beads allows for their overlapping and, therefore, it is possible to set much longer timesteps and larger simulation boxes than in typical molecular dynamics (MD) simulations. The target of DPD is, in fact, the description of the hydrodynamics at the mesoscopic scales where thermal fluctuations are relevant.

In the original DPD formulation, each bead experiences not only conservative forces, but also dissipative and random forces acting along the separation distance between two beads, satisfying the fluctuation-dissipation theorem (FDT) and working as a thermostat[13]. However, although standard DPD gives good results in equilibrium simulations, it has been shown that the DPD method fails in recovering the transport properties of real fluids[14]. Two important transport properties are grouped into the Schmidt number, Sc, defined as the ratio between the fluid kinematic viscosity, ν, and the self-diffusion coefficient, $\mathscr{D}$:

$$Sc = \frac{\nu}{\mathscr{D}}. \tag{1}$$

The Schmidt number is a measure of the relative importance between fluid particle diffusion and momentum diffusion. For a typical liquid, the Schmidt number is $O(10^3)$, meaning that the momentum is usually transported more efficiently than fluid particles themselves, because of the caging effect of the interparticle potential. In their work, Groot and Warren[14] showed that the original DPD scheme results in Schmidt number of $O(1)$, with a dependence on the various DPD parameters that can be expressed as:

$$Sc \sim \gamma^2 \rho^2 r_c^8, \tag{2}$$

where γ is the dissipative parameter, ρ is the density of DPD fluid and r_c is the cutoff radius for interparticle forces. However, even if these parameters strongly affect the Schmidt number simply by increasing them, also the computational costs would increase either directly, or indirectly by having to decrease the timestep in order to maintain the simulation stability[14].

Since the pioneering work of Groot and Warren, many researchers investigated the possibility to describe high Schmidt number fluids with DPD. One of the proposed approaches was to modify the weighting function for the dissipative and random forces, applying the so-called generalized weighting function (GWF)[10,15,16], which still satisfies the FDT as standard DPD. The effect of this modification was the increase of the fluid viscosity, allowing to investigate higher Sc numbers than standard DPD with a comparable computational effort. Another modification to the weighting function was proposed by Yaghoubi and coworkers[17]. The drawback of these approaches, as in standard DPD, is the lack of shearing dissipation which has a great impact on the resulting viscosity of the simulated DPD fluid. In fact, with the standard DPD method, the dissipative force vanishes, no matter how close the two particles are, whenever the relative velocity between two beads is perpendicular to their distance. To overcome this issue, Junghans and coworkers proposed an extended DPD version in which the shearing dissipation is considered, by evaluating the perpendicular contribution of dissipative and random forces[18]. As explained in their work, this extension can be interpreted as a different thermostat for DPD, a transverse DPD thermostat, that is able to describe the damping perpendicular to the interatomic axis, mimicking the shear of those degrees of freedom that were integrated out in the CGing procedure. This extended DPD makes possible to increase Sc number because the shearing dissipation is considered. In fact, the dynamical properties, both viscosity and diffusion coefficient, are very sensitive to the damping perpendicular to the interatomic axis. Moreover, in the case of transverse DPD the

3

friction coefficient and the cutoff radius strongly affect the Schmidt number. From a qualitative point of view the influence of these parameters is quite similar. Increasing r_c or γ increases the mean value of the dissipative force applied to the beads, resulting in a higher viscosity and a lower diffusion constant. In a simulation with the Transverse DPD thermostat, the effect of these two parameters on the Sc number is more accentuated than in Eq. 2, which was derived from Groot and Warren[14] in the case of standard DPD. In the case of the transverse DPD, another relationship should be derived including the perpendicular contribution of dissipative and random forces in the derivation. However, it should be noted that these analytical relationships are derivated neglecting contributions from the conservative forces. Therefore, this method results in higher Sc number than the standard DPD while preserving within an acceptable error bar hydrodynamics. In fact, by using the transverse DPD thermostat, Galilei invariance remains valid by construction while hydrodynamics is conserved within acceptable error bar, while the local angular momentum is not conserved, due to the presence of non-central forces acting between particles. Nevertheless, according to simulation results showed in the work of Junghans and coworkers, these angular momentum fluctuations cancel out on average and hence the total angular momentum of the system is almost a conserved quantity[18]. For this reason, in this work the requirement on angular momentum conservation, which is particularly important when non-equilibrium simulations are used to measure the fluid viscosity, can be relaxed since equilibrium simulations are performed. In this sense, a more complete method, called Fluid Particle Model (FPM), was proposed by Español[19], in which both shearing dissipation and conservation of angular momentum are considered. Pan and coworkers[15] proposed a modified version of FPM, which is more similar to the transverse DPD thermostat and standard DPD method, including all the modifications which have an impact on the Sc number of the investigated fluid, such as the GWF and the shearing dissipation, in a framework that preserves the total angular momentum. With this approach, the beads experience not only parallel and shear dissipation, but also a rotational damping contribution which can be properly evaluated only if the total angular momentum is conserved. This additional contribution has an impact on the resulting fluid viscosity, as shown by Krafnik and Garcia[20]. In their work Krafnik and Garcia pointed out the influence of the different DPD parameters on the resulting Sc number of the simulated DPD fluid. However, the major drawback of this approach is the computational time, which is significantly higher than standard or extended DPD due to the evaluation of the rotational damping contribution.

Therefore in this work, we decided to investigate the performance of the transverse DPD ther-

mostat in simulating high Sc number fluids with equilibrium simulations, aiming at finding the DPD parameters capable of proper recovering the rheological behavior of liquid water at room temperature and pressure. Moreover, special attention was devoted to a peculiar aspect, which is often overlooked, namely the calculation of the fluid viscosity from simulations. In general, the methods for the evaluation of the viscosity from atomistic simulations are divided into two groups: equilibrium and non-equilibrium methods. To the first category belong methods such as Green-Kubo and Einstein-Helfand, while to the latter one the reverse non-equilibrium molecular dynamics (RNEMD), the periodic Poiseuille flow method and the periodic Lees-Edwards flow method. Even though it was shown that non-equilibrium methods for viscosity evaluation are generally more accurate and stable[21], they require subjecting the investigated system under an extreme shear rate, impossible to reach in real systems, while it is not feasible to explore low shear rates, since the effect of the shear is covered by the dissipative and random forces. When Newtonian fluids are investigated, non-equilibrium measurement technique can be used, since the shear rate is independent of the shear stress. On the contrary in the case of non-Newtonian fluids, such as polymer or surfactant solutions, the use of non-equilibrium methods would result in viscosity values corresponding to unphysically large shear rates. In addition, applying the non-equilibrium viscosity measurement for self-assembled systems may alter equilibrium morphologies, discriminating the non-equilibrium approaches for the self-assembled systems. Equilibrium methods overcome these issues and allow us to measure the zero-shear viscosity, often presented in experimental studies of non-Newtonian fluids. For this reason, in this work different viscosity estimation methods were tested, but with the aim of finding a reliable equilibrium algorithm that can be used in further studies on the dynamics of polymer or surfactant solutions.

II. DISSIPATIVE PARTICLE DYNAMICS

As previously mentioned, DPD is a CG simulation technique which treats groups of atoms as single particles, often called beads. In the DPD tipically the mass of a single DPD particle, force cutoff radius and thermal energy are taken as respectively mass, time and energy basic units. The viscosity and diffusivity of the system are, thus, not defined explicitly but in terms of these DPD units. Positions and momenta of those interacting beads are then calculated with the following equations:

$$\frac{d\boldsymbol{r}_i}{dt} = \boldsymbol{v}_i, \quad \frac{d\boldsymbol{v}_i}{dt} = \frac{\boldsymbol{f}_i}{m_i},$$ (3)

5

where $\boldsymbol{r}_i$ and $\boldsymbol{v}_i$ are position and velocity of the bead i with mass m_i, respectively. In the case of a simple DPD fluid, the force $\boldsymbol{f}_i$, acting on $i-$th bead, is a sum of three pairwise contributions:

$$\boldsymbol{f}_i = \sum_{j \neq i} (\boldsymbol{F}_{ij}^C + \boldsymbol{F}_{ij}^D + \boldsymbol{F}_{ij}^R). \tag{4}$$

In Eq. (4), the sum runs over the indices of beads contained in the closest vicinity of bead i within a certain cutoff radius. A conservative contribution, $\boldsymbol{F}_{ij}^C$, is a soft-repulsive force acting between two beads i and j is defined as:

$$\boldsymbol{F}_{ij}^C = \begin{cases} a_{ij} \left(1 - \frac{r_{ij}}{r_c^C}\right) \hat{\boldsymbol{r}}_{ij}, & r_{ij} < r_c^C \\ 0, & r_{ij} > r_c^C \end{cases} \tag{5}$$

where a_{ij} denotes a maximum repulsion between beads i and j, $r_{ij} = |\boldsymbol{r}_{ij}| = |\boldsymbol{r}_i - \boldsymbol{r}_j|$ is the separation distance between a pair of the beads, $\hat{\boldsymbol{r}}_{ij} = \boldsymbol{r}_{ij}/r_{ij}$ is the unit vector of the bead-bead separation distance and r_c^C is the cutoff radius for the conservative interactions. Dissipative and random forces, $\boldsymbol{F}_{ij}^D$ and $\boldsymbol{F}_{ij}^R$, respectively, introduce viscous drag and thermal noise to the system, respectively, and act together as a thermostat.

In the standard DPD thermostat, as originally introduced[12], employed in many prior works[22–25], the dissipative and random forces act, similarly as the conservative force, along the bead-bead separation distance. However in this work, the extended DPD thermostat, proposed by Junghans and coworkers[18], was used. In this approach the standard DPD thermostat is combined with the transverse DPD thermostat acting in the plane perpendicular to the bead-bead separation distance. The expressions for general dissipative and random forces can then be written as

$$\boldsymbol{F}_{ij}^D = -\gamma_\| w_\|^2(r_{ij})(\hat{\boldsymbol{r}}_{ij} \cdot \boldsymbol{v}_{ij})\hat{\boldsymbol{r}}_{ij} - \gamma_\perp w_\perp^2(r_{ij})(\boldsymbol{I} - \hat{\boldsymbol{r}}_{ij}\hat{\boldsymbol{r}}_{ij}^T)\boldsymbol{v}_{ij}, \tag{6}$$

$$\boldsymbol{F}_{ij}^R = \sigma_\| w_\|(r_{ij})\frac{\xi_{ij}}{\sqrt{\Delta t}}\hat{\boldsymbol{r}}_{ij} + \sigma_\perp w_\perp(r_{ij})(\boldsymbol{I} - \hat{\boldsymbol{r}}_{ij}\hat{\boldsymbol{r}}_{ij}^T)\frac{\boldsymbol{\xi}_{ij}}{\sqrt{\Delta t}}. \tag{7}$$

Here $\gamma_\|$ and $\gamma_\perp$ are parallel and perpendicular dissipative parameters, respectively, analogously $\sigma_\|$ and $\sigma_\perp$ are parallel and perpendicular noise parameters, $w_\|(r_{ij})$ and $w_\perp(r_{ij})$ are weighting functions for the parallel and perpendicular parts of $\boldsymbol{F}_{ij}^D$ and $\boldsymbol{F}_{ij}^R$, $\boldsymbol{v}_{ij} = \boldsymbol{v}_i - \boldsymbol{v}_j$, ξ_{ij} and $\boldsymbol{\xi}_{ij}$ are scalar and vector random numbers, respectively, with zero mean value and unit variance, $\boldsymbol{I}$ is the identity second-rank matrix and Δt is the simulation timestep. The dissipative and noise parameters are related to each other in order to satisfy the fluctuation-dissipation theorem (FDT):

$$\sigma_\alpha = \sqrt{2k_B T \gamma_\alpha}, \quad \alpha \in \{\|,\perp\}, \tag{8}$$

where k_B denotes the Boltzmann constant and T the system temperature. This paper utilizes, instead of the traditional quadratic scheme usually adopted[22], as by Junghans and coworkers, the GWF, introduced by Fan and coworkers[10] as previously mentioned, but with the introduction of a Dissipative cutoff radius, r_c^D. This parameter doesn't change the range of conservative force and consequently has no influence on the nature of the phase assumed by the simulated system, described by the radial distribution function (RDF). Infact, the equilibrium behaviour of the system is determined solely by conservative forces because the time average of the dissipative and fluctuation forces is zero.[22–24] Conversely, it is important for the description of the transport properties. So we use the following GWF to improve on the Schmidt number for the system:

$$w_\alpha(r_{ij}) = \left(1 - \frac{r_{ij}}{r_c^D}\right)^{s_\alpha}, \quad \alpha \in \{\|,\perp\}, \tag{9}$$

and its exponent, $s_\alpha \in (0,1]$, plays an important role in modeling of dynamic properties of a DPD fluid. In this work we do not study the exponents separately but we simply assume that $s_\| = s_\perp = s$ and consequently $w_\|(r_{ij}) = w_\perp(r_{ij}) = w(r_{ij})$.

III. EVALUATION OF TRANSPORT COEFFICIENTS IN DPD SIMULATIONS

The estimation of transport coefficients in DPD simulations takes place with numerical techniques developed for atomistic simulations. We review them in the following sections.

A. Self-diffusivity

The self-diffusion coefficient in DPD simulations can be calculated either by the Einstein relation or with the Green-Kubo approach[26]. In the first method, the self-diffusion coefficient, proportional to the mean-square displacement (MSD) of the beads and for the bulk phase, is expressed as follows:

$$\mathscr{D} = \lim_{t \to +\infty} \frac{< [\boldsymbol{r}(t_0 + t) - \boldsymbol{r}(t_0)]^2 >}{6t}, \tag{10}$$

where $< \cdots >$ denotes an ensemble average. While the Green-Kubo approach relates the self-diffusion coefficient to the velocity auto-correlation function (VACF) and reads as follows:

$$\mathscr{D} = \frac{1}{3} \int_0^{+\infty} < \boldsymbol{v}(t_0) \cdot \boldsymbol{v}(t_0 + t) > dt. \qquad (11)$$

It is worth noting that from a theoretical point of view both approaches are equivalent and the choice of one over the other should not give different results. On one side the Einstein relation uses the MSD, which can be easily evaluated from DPD simulations, whereas on the other side the Green-Kubo approach requires the calculation of the time integral of the VACF, which can be tricky from a numerical point of view as seen below. For this reason in this work, we used the Einstein relation to calculate the self-diffusion coefficient.

B.   Viscosity

In principle, we can distinguish between two classes of methods for the calculation of shear viscosity in MD/DPD. The first one, usually denoted as non-equilibrium molecular dynamics (NEMD), is based on the measurement of the system response after imposing on it either a velocity gradient, $\frac{(\partial u_x)}{\partial z}$, (by Lees-Edwards boundary condition[27] or boundary-driven shear flow) or a momentum flux (RNEMD)[28] and/or a body force (Poiseuille method)[29]. The viscosity is then calculated, $\mu = \nu/\rho$, from the generalized-Newton-viscosity law:

$$j_z(p_x) = -\mu \frac{(\partial u_x)}{\partial z}, \qquad (12)$$

where $j_z(p_x)$ is the flux of the $x-$component of the momentum, p_x, in the $z-$direction. The second class of methods calculates the viscosity by means of an equilibrium simulation, using either the Green-Kubo approach or the Einstein-Helfand relation. As previously mentioned, in this paper we are interested in the use of equilibrium methods to estimate the viscosity from the simulation. However, the RNEMD method by Müller-Plathe[28] is used as a benchmark to double-check and verify the evaluation of viscosity by the equilibrium methods.

1.   Green-Kubo approach

Similarly to the self-diffusion coefficient calculations, Green-Kubo[30,31] relation allows to calculate the viscosity by integrating the autocorrelation function. In this case, however, the stress autocorrelation function (SACF) is used:

8

$$\mu = \frac{V}{k_B T} \int_0^{+\infty} < \sigma_{\alpha\beta}(t_0)\sigma_{\alpha\beta}(t_0+t) > dt, \quad (\alpha \neq \beta), \tag{13}$$

where V is the system volume and $\sigma_{\alpha\beta}$ is the off-diagonal component of the stress tensor. In DPD simulations, the stress tensor can be evaluated by the Irving-Kirkwood formula

$$\sigma_{\alpha\beta}(t) = \frac{1}{V}\sum_i \sum_{j<i} r_{ij,\alpha}(t)F_{ij,\beta}(t) + \frac{1}{V}\sum_i m v_{i,\alpha}(t)v_{i,\beta}(t) \tag{14}$$

where $F_{ij,\beta} = F_{ij,\beta}^C + F_{ij,\beta}^D + F_{ij,\beta}^R$, and subscripts α and β are reserved for vector or tensor indices while subscripts i and j for bead indices.

2. Einstein-Helfand approach

Another equilibrium method for calculating viscosity was proposed by Helfand[32] and is analogous to the Einstein (MSD) approach for evaluating the self-diffusion coefficient:

$$\mu = \lim_{t\to+\infty} \frac{V}{2k_B T} < [G_{\alpha\beta}(t) - G_{\alpha\beta}(0)]^2 > \quad (\alpha \neq \beta) \tag{15}$$

where $G_{\alpha\beta}$ is the Helfand moment given by:

$$G_{\alpha\beta}(t) = \sum_i m_i r_{i,\alpha}(t)v_{i,\beta}(t). \tag{16}$$

Since the Einstein-Helfand method is equivalent to the Green-Kubo approach, it can also be expressed in terms of the Irving-Kirkwood stress tensor as follows:

$$G_{\alpha\beta}(t) = G_{\alpha\beta}(0) + \int_0^t \sigma_{\alpha\beta}(\tau)d\tau. \tag{17}$$

3. Non-Equilibrium method

As mentioned above, RNEMD method, originally introduced by Müller-Plathe[28], is based on imposing a momentum flux on the system and then calculating the velocity gradient in order to measure the viscosity of the fluid. It is conducted in the way that the system (a periodic box) is divided into a finite number of layers perpendicular to the $z-$direction. Then, a bead with the largest momentum in the $x-$direction is chosen from the top layer, as well as a bead with the
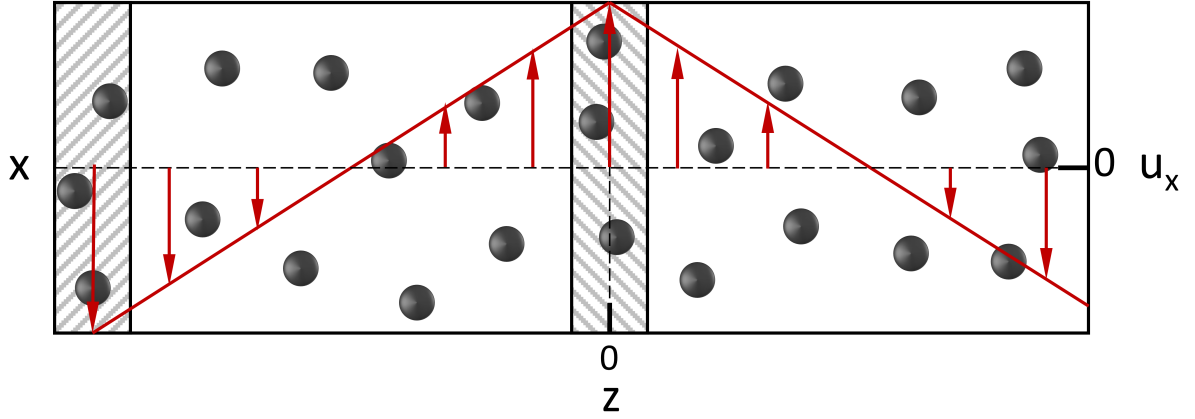
FIG. 1. Schematic representation of the RNEMD method. Velocity field is represented by red arrows.

smallest momentum in the $x-$direction from the middle layer. The momenta of both the beads are swapped. The momentum flux created in this way can be controlled by changing the rate of the momentum swaps. Fig. 1 shows the schematic representation of the simulation box with the velocity profile imposed by RNEMD method.

The momentum flux is then calculated by using the total transferred momentum, P_x, over a time interval, Δt, as follows:

$$j_z(p_x) = \frac{P_x}{2tL_xL_y} \tag{18}$$

where L_x and L_y are box lengths in the $x-$ and $y-$directions, respectively. The factor 2 in the denominator arises because the momentum is transferred in two directions - above and below the middle layer. Due to the momentum flux imposed by the momenta swap, the mean temperature of the domain deviates from the initially specified value and, therefore, the use of a smaller time step and of an additional thermostat may be required when RNEMD method is used. In this work, we used $\Delta t = 0.001$ and the Berendsen thermostat as additional thermostat. In addition, this method has three parameters to be specified by a user: (i) the number of momenta pairs to exchange - usually set to one, (ii) the number of layers in which the domain is divided and which depends on the size of the computational domain, and (iii) the frequency of momentum swap which has a significant influence on the development of the linear velocity profile inside the box. While the first two parameters are usually selected without any issues, it may require a few attempts to find the proper value for the frequency of the momentum swap[28]. Fig. 2 displays as an example the velocity profiles for different momentum exchange frequencies, showing a clear linear velocity profiles for a momentum swap every 25 and 50 timesteps.
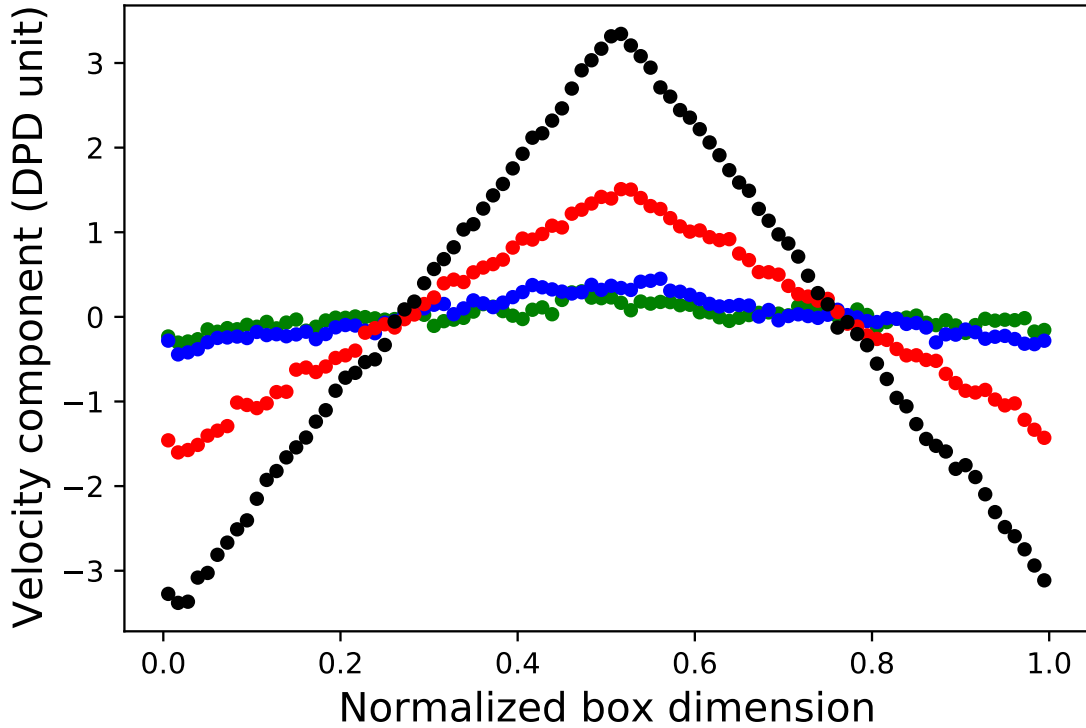
FIG. 2. Velocity profile for different momentum exchange frequencies. Black circles: momentum swap every 25 timesteps. Red circles: momentum swap every 50 timesteps. Blue circles: momentum swap every 500 timesteps. Green circles: momentum swap every 2000 timesteps.

IV. SIMULATION DETAILS

All simulations were performed by using the open-source software LAMMPS[33] with our newly developed LAMMPS `pair_style` for the general dissipative and random forces. DPD fluid was represented by single beads with different degrees of CGing, N_m, which affect the evaluation of the repulsion parameter a of the conservative force, i.e.,

$$a = \frac{N_m \kappa^{-1} - 1}{0.2\rho} k_B T, \tag{19}$$

where N_m corresponds to the number of real molecules per bead, κ^{-1} is the inverse of the dimensionless isothermal compressibility of DPD fluid (e.g., $\kappa^{-1} = 16$ for water) and ρ is the DPD number density corresponding to the number of beads inside a volume of $(r_c^C)^3$. All the equilibrium simulations were performed in a cubic box of the length equal to 15 DPD length units with periodic boundary in all directions, considering r_c^C as the DPD length unit. In cases of RNEMD

11

simulations, the box was a cuboid of size $15 \times 15 \times 45$ DPD length units to capture the velocity gradient in the direction of transferred momentum. The system bead density and system temperature were the same for all the cases and set to $\rho = 3$ and $k_B T = 1$. DPD equations of motion were integrated by using the velocity-Verlet algorithm, proposed by Groot and Warren[14], and used in several prior studies[22,34], with Δt set such that temperature fluctuations were lower than about 3% of $k_B T$. This results in $\Delta t = 0.01$ in the case of equilibrium simulations (apart from some specific test cases highlighted below), and $\Delta t = 0.001$ for non-equilibrium cases. The simulation time statistics were collected within $5 \cdot 10^6$ timesteps. Regarding the calculation of the viscosity with the Green-Kubo approach, it is worth mentioning that LAMMPS uses an approximate algorithm to evaluate SACF. First, the algorithm makes use of the ergodic hypothesis to evaluate the ensemble average as a time integral, and for this reason the final simulation time needs to be sufficiently long to carry out a correct estimation. Then, the SACF is not evaluated according to its definition, since it would be too expensive from the computational point of view. Instead, the SACF averages are computed every N_{freq} timesteps and only a limited data set is actually employed in the SACF evaluation, namely the data points correlated every $N_{ev}-$th timestep for $N_{ev} \cdot (N_{rep} - 1)$ timesteps. For further details on this algorithm readers are referred to the LAMMPS code[33]. Therefore, the choice of N_{ev}, N_{rep} and N_{freq} is critical in the proper evaluation of SACF and, in general, in the viscosity evaluation. After numerous tests performed, we found that by selecting $N_{ev} = 1$, $N_{freq} = 1,000$ and $N_{rep} = 1,000$, the best results are obtained in the evaluation of the SACF. In the cases where $\Delta t = 0.005$, N_{freq} and N_{rep} are taken equal to 2000 to be consistent in the evaluation of the SACF.

V. RESULTS AND DISCUSSION

A. Robust viscosity evaluation procedure

The challenge for the Green-Kubo viscosity calculation stands mainly in the numerical evaluation of the time integral of the SACF from time $t = 0$ up to $+\infty$. A first issue is related to the fact that the SACF is numerically evaluated at each simulation timestep, and after a first clear decaying trend the values of the SACF oscillate around zero with a certain noise, assuming also negative values. An example of this well-known behavior[30], is reported in Fig. 3. Therefore, the calculation of such time integral with a simple trapezoidal rule is affected by the tail oscillations.

To overcome this issue, we tested several procedures. A first attempt was to use a procedure
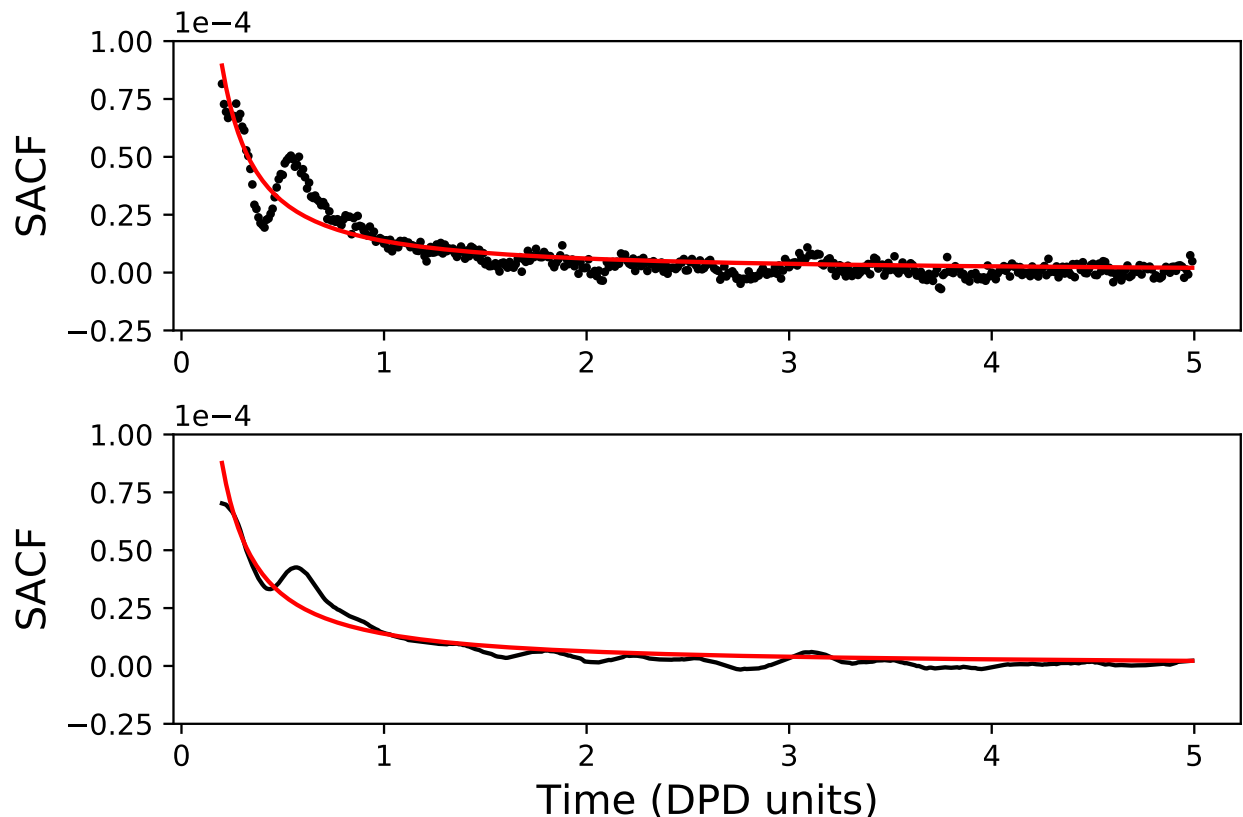
12

FIG. 3. Two different representations of the tail of the same SACF. Top: procedure A. Black circles: points of the SACF. Red line: power-law fit. Bottom: procedure B. Black line: SACF after a moving average filter. Red line: power-law fit..

proposed by Jung and Schmid[35]. The procedure involves the numerical integration by using the trapezoidal rule until the SACF values reached about 1% of their initial values. Then, the tail is fitted using a power-law, i.e.: At^{-B}, and integrated analytically. This first will be denoted as "Procedure *A*" in the following. An alternative is the use of a moving average filter to smooth out the tail oscillations. This involves the choice of the moving average span and then performing the power-law fitting. This is denoted as "Procedure *B*". Also in Procedure *B* the analyzed tail starts at about 1% of initial values of SACF. After preliminary tests on the value of the moving average span, the best result was obtained with an interval of 20 timesteps. Fig. 3 shows examples of Procedure A and Procedure B for a generic DPD simulation.

However, a second issue associated with the power-law fitting procedures must be addressed. In fact, the fitted power-law always approaches zero slower than the actual numerical value of the SACF, which oscillates between positive and negative values when the power-law fit has not reach its asymptotic value. For this reason, we tried to use two approaches for the analytical integration

13

TABLE I. Viscosity values (in DPD unit) calculated with various approaches. Procedure A: power-law fitting. Procedure B: moving average filter before power-law fitting. The superscripts 1 and 2 correspond respectively to a final integration time of $N_{rep} \cdot \Delta t$ and infinite. Procedure C: cumulative integral. E-H and RNEMD refers to Einstein-Helfand and Muller-Plate methods.

$\gamma_\parallel$	A^1	A^2	B^1	B^2	C	E-H	RNEMD
4.5	0.8535	0.8846	0.8706	0.9399	0.860±0.002	0.847	0.860
9	0.9699	1.0018	0.9892	1.0613	0.957±0.004	0.923	0.930
15	1.1128	1.1468	1.1308	1.2065	1.065±0.002	1.071	1.055

of the fitted power-law. In the first approach, the final integration time is the final SACF available from the simulation post-processing, depending on the N_{rep} and Δt, and is labelled with number 1 in Table I. In the second approach, the analytical integration is carried out up to $+\infty$ and is labelled with the number 2 in Table I. As it can be seen in Table I, the second approach has a significant impact on final viscosity values, which may increase of about 3-8% if the analytical integration up to infinity is carried out. Moreover, the effect of the tail noise is still not quantified by using these procedures.

For this reason, we tried to use an approach based on the calculation of the viscosity cumulative integral function of time, denoted as in what follows as "Procedure C". The idea behind this latter procedure is to evaluate the viscosity by using Eq. (13) progressively extending the integration interval up to the final SACF time. The result of Procedure C should theoretically be a monotonic curve that approaches an asymptotic value that corresponds to the system viscosity. However, this is impossible to reach exactly due to the intrinsic stochastic noise within DPD simulations and an example of such calculation is depicted in Fig. 4. In Fig. 4, viscosity values monotonically increase up to approximately 3 DPD unit time, when the value of the viscosity starts to oscillate around a constant value due to the corresponding oscillations in the SACF. Therefore, we opt to evaluate the system viscosity as the average value of the curve considering only the last 5 DPD time units, avoiding the initial transient period. Moreover, Procedure C is particularly convenient since it allows us to evaluate a coefficient of variation, providing therefore not only the expected viscosity value but also the associate uncertainty.

Table I summarizes the values of the viscosity calculated using various Green-Kubo procedures together with viscosity values obtained by using the Einstein-Helfand and RNEMD methods, which were used as benchmark. The simulations were run using a standard DPD thermostat, so $\gamma_\perp = 0$, and $s = 1$, $r_c^D = 1$ and $N_m = 1$. Results are shown for different values of $\gamma_\parallel$ to see
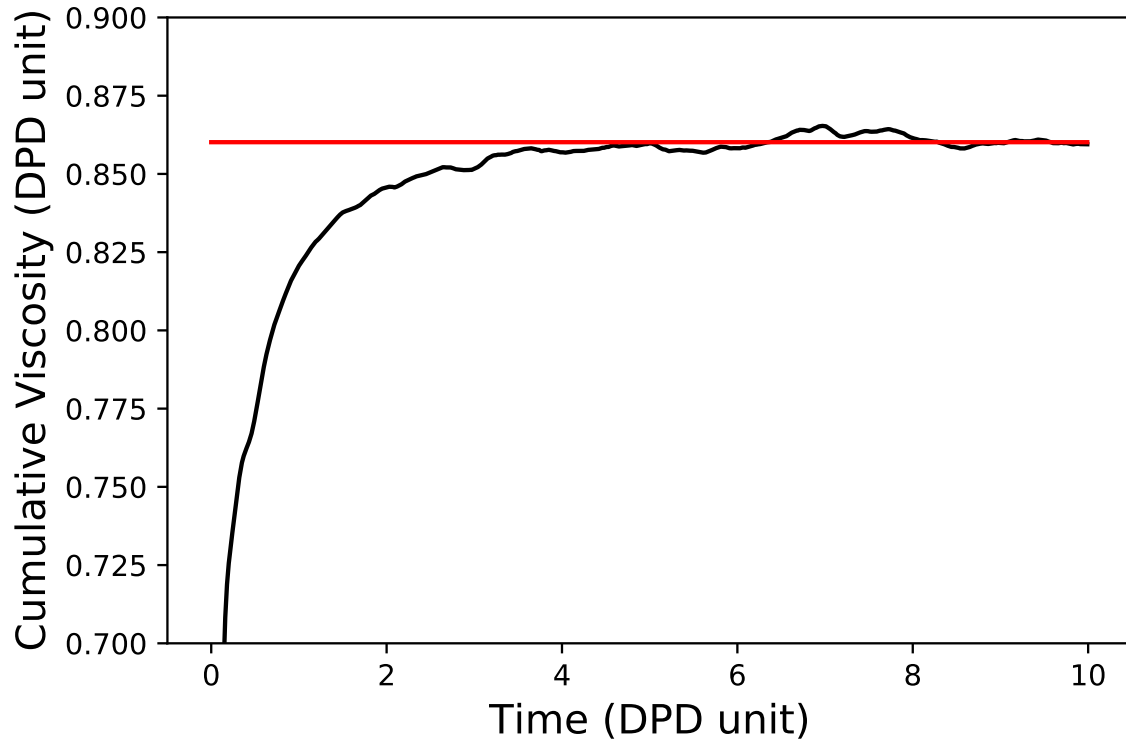
FIG. 4. Cumulative integral of viscosity calculated using the Green-Kubo approach. Black line: viscosity cumulative integral. Red line: mean value and coefficient of variation calculated between $t = 5$ and 10.

the effect of changing one DPD parameter on the viscosity. As it can be seen from Table I, the procedures involving the power-law fit seem to perform quite poorly when compared to other procedures, especially procedure B which has the largest deviations. Procedure C gives instead results that are very close with the other two benchmark methods, and this procedure is then used in the rest of the work. Eventually, it is interesting to see that the coefficient of variation of the viscosity calculation for the reported simulations ranges between 0.2 and 0.4%, which is approximately the range found for all the other evaluations carried out in this work. This is due to the fact that that the whole numerical methodology to evaluate the viscosity of a fluid has an intrinsic accuracy, that derives from the stochastic nature of the DPD model.

B. Schmidt number scaling

Once a reliable procedure for calculating the viscosity was found, the effect of different DPD parameters on SACF and Sc number of DPD fluid was investigated by performing different sim-

ulations, aiming to reproduce the Sc number of water at 25°C equal to about 370. The parameters varied are the dissipative cutoff radius, r_c^D, the weighting function exponent, s, the degree of CGing, N_m, and the dissipative parameters, $\gamma_\parallel$ and $\gamma_\perp$. For simplicity and reducing parameter space, we consider $\gamma_\perp = \gamma_\parallel = \gamma$. Table II provides a summary of all DPD simulations performed.

As expected, the standard choice of DPD parameters reported in the first row of Table II, results in a low Sc number, even if the transverse DPD thermostat is used. Moreover, the Sc number does not increase significantly by reducing the GWF exponent s, unless the degree of CGing N_m is increased as well. In Fig. 5, we can see the reason of this trend: the SACF goes to zero more rapidly when the degree of CGing is small, regardless of the value of the weighting function exponent, resulting therefore in lower viscosity values according to Eq. (13). This means that the conservative force parameter a has a clear influence on the resulting viscosity and self-diffusion coefficient, since N_m is an input to evaluation of a. In fact, by using a higher degree of CGing, the beads in a DPD simulation tend to move less and to exchange more momentum with the surrounding beads, behaving more like a real liquid[36]. Furthermore, as it will be shown in the following, the choice of N_m equal to 10 (i.e., $a = 265$) gives an RDF indicative of the liquid state, as displayed in Fig. 9. Conversely, for $N_m > 10$ ($a > 265$) the radial distribution function (RDF) may present secondary peaks revealing the presence of a crystalline structure[37]. Another interesting aspect to note is an increase of noise in the SACF, evident in Fig. 5 when a lower value s is investigated. Nevertheless, the resulting viscosities have a coefficient of variation in the same range as in all the other investigated cases, between 0.2 up to 0.8%, confirming the validity of the proposed methodology to assess the rheological properties of a DPD fluid.

Fig. 6 shows the influence of the other DPD parameters on the SACF. A larger area below the curve corresponds to a higher value of the viscosity according to the Green-Kubo approach. From Fig. 6, we can see the following trends. The viscosity increases when the dissipative parameter and dissipative cutoff radius increase, and when the GWF exponent decreases, since these increases/decreases enhance bead momentum dissipation. It is worth mentioning that not all the simulations were run with the same set of all the other DPD parameters and also, the timestep was reduced for the sake of simulation stability when the dissipative cutoff radius was increased.

The effect of the variation of individual DPD parameters on the Sc number is presented in Fig. 7, where s was varied between 1 and 0.125, r_c^D between 1 and 1.8 and γ between 4.5 and 72. Fig. 7 shows that the Sc number can be increased by up to two orders of magnitude. As previously mentioned, we also noticed a strong dependence of Sc number on N_m as depicted in

16

TABLE II. Summary of all DPD simulation performed, including the results in terms of viscosity, self-diffusion coefficient and Schmidt number; all properties are in DPD units. All simulations are carried out with $\rho = 3$. Rows highlighted in bold font are close to the Schmidt number of water at 25°C equal to about 370.

| N_m	s	γ	r_c^D	Δt	ν	$\mathscr{D}$	Sc
1	1	4.5	1	0.01	0.430	0.173	2.489
1	0.5	4.5	1	0.01	1.078	0.075	14.373
1	0.25	4.5	1	0.01	2.446	0.038	64.377
1	0.125	4.5	1	0.01	3.687	0.026	141.82
3	1	4.5	1	0.01	0.748	0.099	7.560
3	0.5	4.5	1	0.01	1.612	0.047	34.291
3	0.25	4.5	1	0.01	2.914	0.026	112.06
3	0.125	4.5	1	0.01	4.919	0.017	289.33
10	1	4.5	1	0.01	3.116	0.029	108.53
10	0.733	4.5	1	0.01	3.949	0.024	166.07
10	0.633	4.5	1	0.01	4.245	0.021	203.12
10	0.533	4.5	1	0.01	5.013	0.018	276.35
10	0.5	4.5	1	0.01	5.021	0.017	290.24
10	0.48	4.5	1	0.01	5.055	0.017	300.38
10	0.46	4.5	1	0.01	5.619	0.016	349.02
10	**0.434**	**4.5**	**1**	**0.01**	**5.890**	**0.016**	**368.54**
10	0.432	4.5	1	0.01	5.950	0.015	384.92
10	0.43	4.5	1	0.01	6.053	0.015	404.09
10	0.42	4.5	1	0.01	6.106	0.015	423.13
10	0.4	4.5	1	0.01	6.253	0.014	444.77
10	0.32	4.5	1	0.01	7.757	0.012	636.88
10	0.3	4.5	1	0.01	7.758	0.011	681.18
10	0.28	4.5	1	0.01	7.834	0.010	725.40
10	0.26	4.5	1	0.01	8.135	0.010	813.46
10	0.25	4.5	1	0.01	8.743	0.010	892.11
10	0.125	4.5	1	0.01	12.13	0.007	1784.1
10	1	9	1	0.01	4.289	0.024	177.00
10	1	18	1	0.01	5.414	0.017	319.96
10	**1**	**20.2**	**1**	**0.01**	**5.880**	**0.016**	**367.70**
10	1	22	1	0.01	5.879	0.015	397.25
10	1	24	1	0.01	6.361	0.014	453.40
10	1	25	1	0.01	6.387	0.014	458.62
10	1	30	1	0.01	7.862	0.012	650.81
10	1	36	1	0.01	7.999	0.010	767.75
10	1	72	1	0.01	15.33	0.005	2797.2
10	1	4.5	1.2	0.005	4.472	0.021	209.19
10	**1**	**4.5**	**1.38**	**0.005**	**5.870**	**0.016**	**366.88**
10	1	4.5	1.4	0.005	5.990	0.015	395.63
10	1	4.5	1.6	0.005	14.32	0.007	1962.1
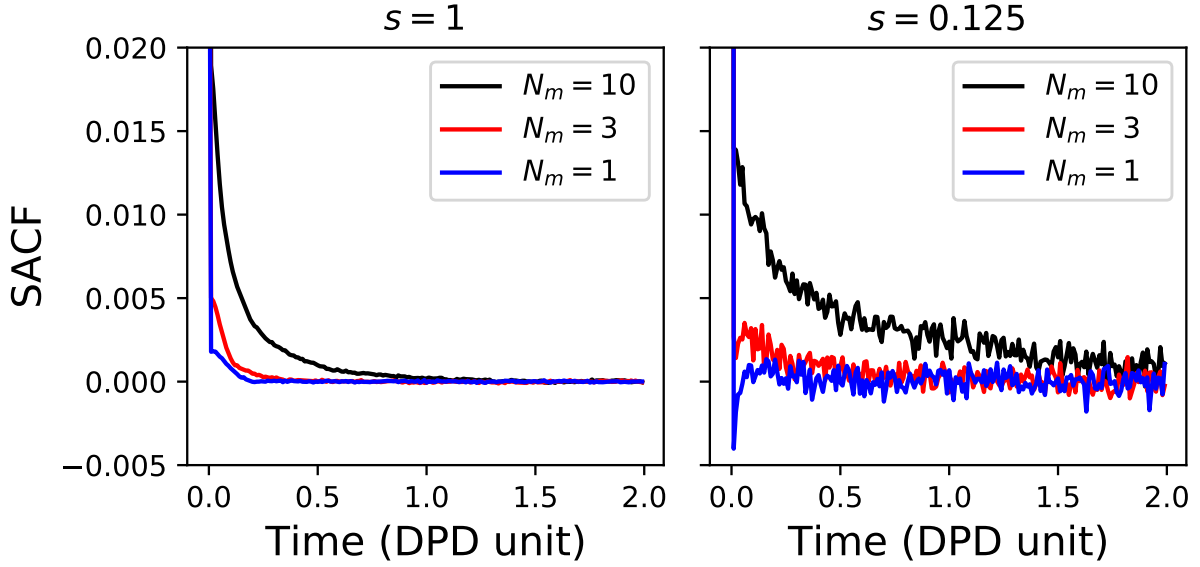
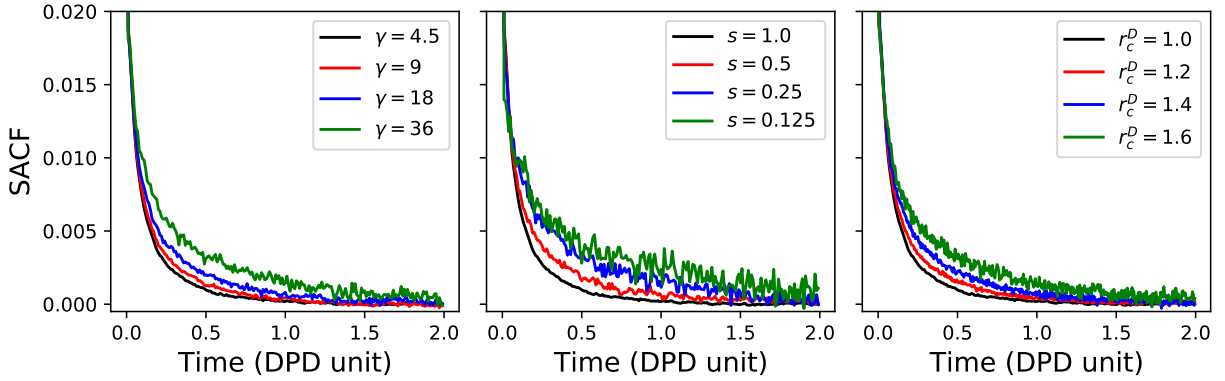FIG. 5. Effect of the degree of CGing, N_m, on the SACF for two different values of the GWF exponent s.

FIG. 6. Effects of the (left) dissipative parameter γ, (center) GWF exponent s and (right) dissipative cutoff radius r_c^D on the SACF.

Fig. 8. Dependencies of the Sc number on the DPD parameters were fit with a single-variable power-law, since the number of performed simulations does not allow for a multi-variable fitting.

C. Tuning water transport properties

In the following, we show in detail the results for the three sets of DPD parameters (highlighted in bold font in Table II), that give a Sc number about 370, which corresponds to the Sc number of liquid water at 25°C. The corresponding simulation results are reported in Table III where we
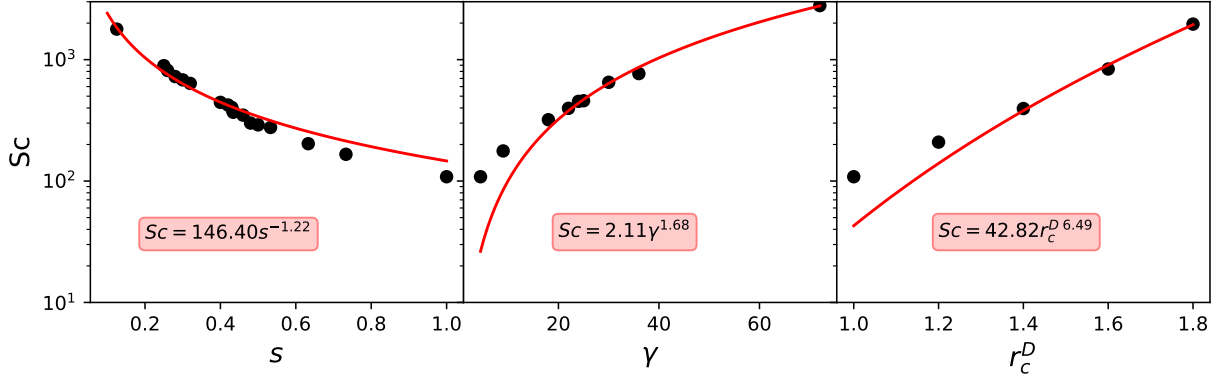
FIG. 7. The Schmidt number as a function of (left) dissipative parameter γ, (middle) GWF exponent s and (right) dissipative cutoff radius r_c^D. Dependencies of the Schmidt number on the DPD parameters were fit to the power-law.
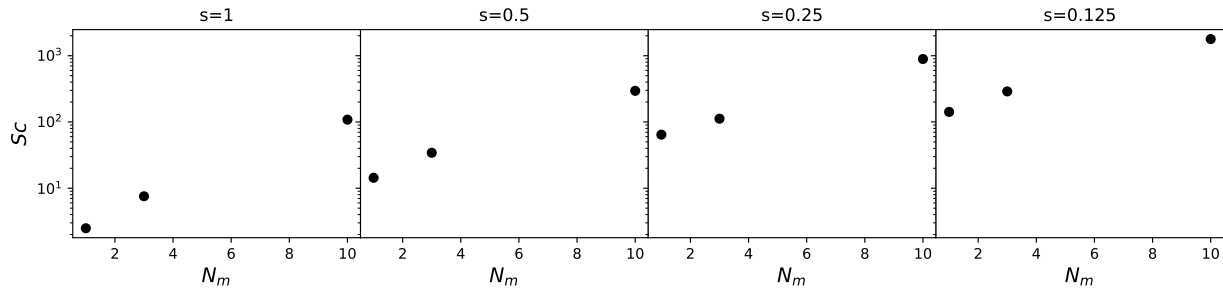

FIG. 8. The Schmidt number as a function of the degree of CGing, N_m, for different values of the GWF exponent s.

compare the viscosity obtained via Green-Kubo approach with that from the Einstein-Helfand and RNEMD methods. We can see that all the viscosities are similar, confirming once again that our procedure based on the Green-Kubo approach can be adopted for evaluating the viscosity. In addition, other aspects are worth to be highlighted. First, the conversion of viscosity and self-diffusion values from DPD units to real units, reported in Table III, gives realistic results for liquid water at 25°C. To evaluate the conversion factors, we adopted the approach of Groot and Rabone[38], in which the value of the characteristic length r_c is estimated from the physical volume occupied by ρN_m water molecules, namely:

$$r_c = 3.107(\rho N_m)^{1/3}, \quad (\text{Å}) \tag{20}$$

19

TABLE III. The properties of DPD fluid corresponding to the three sets of DPD parameters, calibrated against the Schmidt number of liquid water at 25°C equal to about 370.

	Set 1	Set 2	Set 3
s	0.434	1	1
r_c^D	1	1.38	1
γ	4.5	4.5	20.2
Δt	0.01	0.005	0.01
N_m	10	10	10
ρ	3	3	3
v^{DPD} (RNEMD)	5.76	5.26	4.67
v^{DPD} (E-H)	5.74	5.53	5.74
v^{DPD} (G-K)	5.89	5.87	5.88
v (m^2/s)	$0.895 \cdot 10^{-6}$	$0.892 \cdot 10^{-6}$	$0.893 \cdot 10^{-6}$
$\mathscr{D}^{\text{DPD}}$	0.016	0.016	0.016
$\mathscr{D}$ (m^2/s)	$2.43 \cdot 10^{-9}$	$2.43 \cdot 10^{-9}$	$2.43 \cdot 10^{-9}$
Sc	368.54	366.88	367.70
γ^{eff}	4.36	3.90	4.00

the characteristic mass of a bead m using the mass of a water molecule $m_w = 2.992 \cdot 10^{-26}$ kg in the following manner:

$$m = N_m m_w, \tag{21}$$

and the characteristic time by matching the experimental self-diffusion coefficient $\mathscr{D}^{\text{exp}}$ of the liquid water by using the following expression:

$$\tau = \frac{N_m \mathscr{D}^{\text{DPD}} r_c^2}{\mathscr{D}^{\text{exp}}}. \tag{22}$$

The simulation results corresponding to the three sets of DPD parameters are very close to the experimental values of $0.9 \cdot 10^{-6}$ m^2/s for viscosity and $2.4 \cdot 10^{-9}$ m^2/s for the self-diffusion coefficient of the liquid water. This thus indicates that the transverse DPD thermostat can reproduce the proper momentum and mass transport behavior of liquid water, with at least three different sets of DPD parameters. Another confirmation of this behavior can be seen in Fig. 9, which displays the RDFs calculated from the DPD simulations with the three sets of DPD parameters. As it can be seen, the RDFs for all three cases overlap, as expected, since the only contribution that defines its shape is that of conservative interactions, which are identical in all three cases.

Another important parameter reported in Table III is the so-called effective friction coefficient[39],
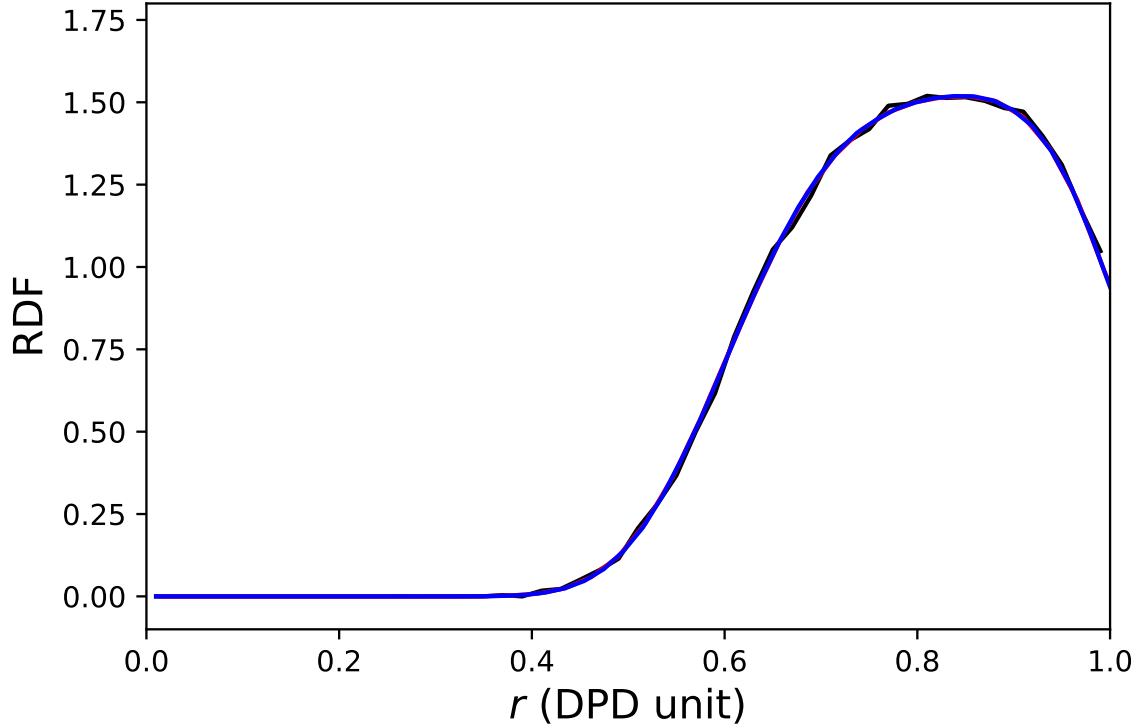
FIG. 9. Radial distribution function evaluated for the three sets of DPD parameters, calibrated against the Schmidt number of liquid water at 25°C equal to about 370. Black line: Set 1, red line: Set 2, blue line: Set 3.

defined as follows:

$$\gamma^{\text{eff}} = \int_0^{r_c^D} \gamma w(r_{ij}) g(r_{ij}) 4\pi r^2 dr_{ij}, \tag{23}$$

where $g(r_{ij})$ is the RDF. The effective friction coefficient is a measure of the overall bead friction and combines the effects of s, r_c^D, γ and implicitly of N_m into one single characteristic quantity. We can see from Table III that values of γ^{eff} for the three sets are rather similar, supporting the following conclusion: sets of parameters (s, r_c^D, γ) having the same γ^{eff} give the same dynamical properties. A last consideration involves the computational time. Set 2 requires more computational resources than the other two cases since Δt for Set 2 is half of Δt for the other cases to keep under control temperature oscillations and to guarantee simulation stability. To allow a consistent comparison of the time statistics for all the three cases, the simulation time was doubled for Set 2. Moreover, a dissipative cutoff radius greater than the conservative cutoff radius in Set 2 decreases the code efficiency, since the use of different cutoff radius values for the different forces significantly increases the computational time. Therefore, changing γ or s to increase the Sc number has

21

no or minimal effect on the computational time and simulation stability, unlike tuning r_c^D which can be rather computational demanding.

VI. CONCLUSIONS

The main conclusions of this work are the following.

The viscosity coefficient estimated via the Green-Kubo approach is comparable with that obtained by using other methods (i.e., Einstein-Helfand equilibrium and non-equilibrium RNEMD methods) with the advantage that there is no limitation on its usage for equilibrium simulations. This becomes crucial for viscosity prediction in self-assembled non-Newtonian systems. Moreover, the proposed method of treating the noise of the SACF tail is capable of giving not only the mean viscosity value, but also the uncertainty of the numerical procedure associated with the viscosity evaluation. In this work, we show that such uncertainty is lower or comparable to the uncertainty of the experimental measurements.

The transverse DPD thermostat can be used to simulate high Sc number fluids, especially when the degree of CGing N_m higher than the standard N_m is adopted. The dependence of the Sc number on the dissipative parameter γ, the dissipative cutoff radius r_c^D and the GWF exponent s were also explored and quantified.

We observed that three different sets of DPD parameters lead to the same Sc number, RDF and effective friction coefficient. Essentially, we obtained the same fluid with the same rheological behavior with three different sets of DPD parameters. Moreover, we also found that increasing r_c^D to increase the Sc number of the fluid is computational costly when compared to changing γ and s.

ACKNOWLEDGMENTS

AUTHOR CONTRIBUTIONS

All authors contributed to the study conception and design. Software programming, data collection and analysis were performed by Nunzia Lauriello. The first draft of the manuscript was written by Juliusz Kondracki and all the authors iteratively corrected and contributed to the final version of the manuscript.

DATA AVAILABILITY

The data that support the findings of this study are openly available in Zenodo at `http://doi.org/10.5281/zenodo.4721189`.

REFERENCES

[1] M. Karimi, H. Droghetti, and D. L. Marchisio, Macromolecular Symposia **360**, 108 (2016).

[2] M. Karimi, D. Marchisio, E. Laurini, M. Fermeglia, and S. Pricl, Chemical Engineering Science **178**, 39 (2018).

[3] P. Ferkl, M. Karimi, D. L. Marchisio, and J. Kosek, Chemical Engineering Science **148**, 55 (2016).

[4] A. D. Lavino, N. D. Pasquale, P. Carbone, and D. L. Marchisio, Chemical Engineering Science **171**, 485 (2017).

[5] R. Mao, M.-T. Lee, A. Vishnyakov, and A. V. Neimark, The Journal of Physical Chemistry B **119**, 11673 (2015).

[6] H. Droghetti, I. Pagonabarraga, P. Carbone, P. Asinari, and D. Marchisio, The Journal of Chemical Physics **149**, 184903 (2018).

[7] R. Pasquino, H. Droghetti, P. Carbone, S. Mirzaagha, N. Grizzuti, and D. Marchisio, Soft Matter **15**, 1396 (2019).

[8] A. D. Lavino, P. Carbone, and D. Marchisio, The Canadian Journal of Chemical Engineering **98**, 1868 (2020).

[9] X. Fan, N. Phan-Thien, N. T. Yong, X. Wu, and D. Xu, Physics of Fluids **15**, 11 (2003).

[10] X. Fan, N. Phan-Thien, S. Chen, X. Wu, and T. Y. Ng, Physics of Fluids **18**, 063102 (2006).

[11] G. Boccardo, A. Buffo, and D. Marchisio, Chemical Engineering & Technology **42**, 1654 (2019).

[12] P. J. Hoogerbrugge and J. M. V. A. Koelman, Europhysics Letters (EPL) **19**, 155 (1992).

[13] P. Español and P. Warren, Europhysics Letters (EPL) **30**, 191 (1995).

[14] R. D. Groot and P. B. Warren, The Journal of Chemical Physics **107**, 4423 (1997).

[15] W. Pan, I. V. Pivkin, and G. E. Karniadakis, EPL (Europhysics Letters) **84**, 10012 (2008).

[16] Z. Li, Y.-H. Tang, H. Lei, B. Caswell, and G. E. Karniadakis, Journal of Computational Physics **265**, 113 (2014).

[17] S. Yaghoubi, E. Shirani, A. R. Pishevar, and Y. Afshar, EPL (Europhysics Letters) **110**, 24002 (2015).

[18] C. Junghans, M. Praprotnik, and K. Kremer, Soft Matter **4**, 156 (2008).

[19] P. Español, Physical Review E **57**, 2930 (1998).

[20] R. C. Krafnick and A. E. García, The Journal of Chemical Physics **143**, 243106 (2015).

[21] S. D. Stoyanov and R. D. Groot, The Journal of Chemical Physics **122**, 114112 (2005).

[22] S. Chen, N. Phan-Thien, B. C. Khoo, and X. J. Fan, Physics of Fluids **18**, 1 (2006).

[23] P. D. Palma, P. Valentini, and M. Napolitano, Physics of Fluids **18**, 1 (2006).

[24] Z. Li and G. Drazer, Physics of Fluids **20**, 1 (2008).

[25] N. Mai-Duy, N. Phan-Thien, T. Nguyen, and T. Tran-Cong, Physics of Fluids **32**, 1 (2020).

[26] J.-P. Hansen and I. R. McDonald, *Theory of Simple Liquids* (Academic Press, Amsterdam, Netherlands, 2013).

[27] A. W. Lees and S. F. Edwards, Journal of Physics C: Solid State Physics **5**, 1921 (1972).

[28] F. Müller-Plathe, Physical Review E **59**, 4894 (1999).

[29] J. A. Backer, C. P. Lowe, H. C. J. Hoefsloot, and P. D. Iedema, The Journal of Chemical Physics **122**, 154503 (2005).

[30] M. S. Green, The Journal of Chemical Physics **22**, 398 (1954).

[31] R. Kubo, Journal of the Physical Society of Japan **12**, 570 (1957).

[32] E. Helfand, Physical Review **119**, 1 (1960).

[33] S. Plimpton, A. Kohlmeyer, A. Thompson, S. Moore, and R. Berger, "Lammps stable release 29 october 2020," (2020), https://doi.org/10.5281/zenodo.4157471.

[34] H. Reddy and J. Abraham, Physics of Fluids **21**, 1 (2009).

[35] G. Jung and F. Schmid, The Journal of Chemical Physics **144**, 204104 (2016).

[36] W. Dzwinel and D. A. Yuen, International Journal of Modern Physics C **11**, 1 (2000).

[37] I. V. Pivkin and G. E. Karniadakis, The Journal of Chemical Physics **124**, 184101 (2006).

[38] R. Groot and K. Rabone, Biophysical Journal **81**, 725 (2001).

[39]F. Lahmar and B. Rousseau, Polymer **48**, 3584 (2007).